Low Velocity Impact of an Elastic Plate Resting on Sand

H. L. Chen

W. Lin

L. M. Keer
Fellow ASME.

S. P. Shah

Northwestern University
Evanston, IL 60208

This article describes the measurement and analysis of plate and soil response under low velocity impact. A free-drop impact system was developed to generate the dynamic loading on the plate free surface. The radial strain of the target plate, the longitudinal wave speed and the acceleration of the sand were measured. The measured wave speed data were then used to evaluate the elastic constants of the sand. An analysis based on linear elastodynamics was developed for transient waves on a thin plate resting on an elastic half space. The contact stresses and the normal displacements of the plate were taken as unknown functions. The contact between the plate and the half space were assumed frictionless. The experimental results of the radial strain at the bottom of the target plate and the acceleration of the sand beneath the center of the target plate were compared with the analytical solution. The arrival time, the duration, and the magnitude have good correlation between the analysis and experiment. The overall results appear good and provide an understanding of the transmission of impact load through the plate, the interaction between the plate and the sand, and the propagation of the load into the sand.

Introduction

An impulsive loading can be produced by impact where the duration of the impulse is on the order of microseconds. The particular problem of a circular aluminum plate impacted at its center by a steel ball was considered in this study. The contact duration as well as the radius of the contact area were measured and compared with an estimation based upon a Hertzian contact assumption. An excellent review of the works related to experimental studies of wave propagation due to low velocity impact was given by Al-Mousawi (1986). A detailed study of low velocity impact of circular plates was conducted by Greszczuk (1982).

In this paper, an analysis based on linear elastodynamics for the transient waves on an elastic plate which rests on an elastic half space (sand) was developed to understand the applied loading, the interfacial conditions between plate and sand, the validity of the assumed constitutive law for sand and the free field response. Two difficulties addressed in this study were the measurement of the response of the soil, and in adopting an appropriate constitutive law for the soil. The contact stresses and the normal displacements of the plate were taken as unknown functions. The contact between the plate and the half space was assumed frictionless. The measured responses of the radial strains of the target plate, the longitudinal wave speeds, and the accelerations of sand are compared with analytical results to provide a better understanding of how the dynamic load is transmitted through a plate into the soil and how well the elastic half space assumption can be used to model the sand. A review of the analytical approaches used in this study are described as follows.

By assuming the distribution of the contact pressure between the foundation and the soil, Reissner and Sagoci (1944), Quinlan (1954), Sung (1954), Arnold et al. (1955), and Bycroft (1956) considered the dynamic response of a rigid disc placed on an elastic half space based on Lamb's (1904) solution for the elastic half space. Collins (1962), Robertson (1966), Karasudhi et al. (1968), Luco and Westmann (1972), and Veletsos and Verbic (1974) studied the vertical, tangential, and rocking oscillations of a rigid strip on an elastic or viscoelastic half space by solving the actual mixed boundary value problem, either through application of integral transforms or by reduction of the governing equations to an integral equation (essentially a boundary element formulation). A detailed review of pertinent research on the dynamic response of rigid footings can be found in Richard et al. (1970) and Luco et al. (1971, 1987).

The assumption of a rigid foundation may be inappropriate for studying the dynamic interaction between the soil and a structure which has large planar dimensions compared with the incident wave length. The response of an infinite and a semi-infinite flexural plate in smooth contact with an elastic half space subjected to harmonic plane waves was solved by Achenbach et al. (1966), and Freund and Achenbach (1968). In 1973, Oien expanded the motion of the plate in a series of vibrational modes and obtained the response of the plate on the elastic half space using the Bubnov-Galerkin method. In 1978, Lin presented an integral equation approach for the case of a flexible circular plate having a rigid perimeter. Recently, a similar approach was adopted by Iguchi and Luco (1982) to

Contributed by the Applied Mechanics Division of THE AMERICAN SOCIETY OF MECHANICAL ENGINEERS for presentation at the Joint ASCE/ASME Applied Mechanics, Biomechanics, and Fluids Engineering Conference, San Diego, CA, July 9 to 12, 1989.

Discussion on this paper should be addressed to the Editorial Department, ASME, United Engineering Center, 345 East 47th Street, New York, N.Y. 10017, and will be accepted until two months after final publication of the paper itself in the JOURNAL OF APPLIED MECHANICS. Manuscript received by ASME Applied Mechanics Division, December 30, 1987; final revision, April 12, 1988.

Paper No. 89-APM-13.

Table 1 Contact duration and radius of contact area

Velocity of Impactor (m/sec)	Target Plate (Thickness(cm) × Diameter(cm))	Contact Duration T_o(msec)) Measured/Calculated	Contact Radius a(cm) Measured/Calculated
2.95	Steel(2.54 × 15.24)	0.169/0.135	0.160/0.180
2.95	Aluminum(1.27 × 15.24)	0.238/0.174	0.175/0.204
5.06	Steel(2.54 × 15.24)	0.132/0.121	0.263/0.222
5.06	Aluminum(2.54 × 20.32)	0.180/0.156	0.275/0.253

1 Impactor: 4.76 cm diameter steel ball (E52100)
2 Calculated by Hertzian Contact Law

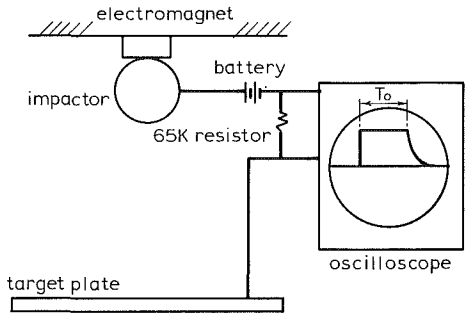

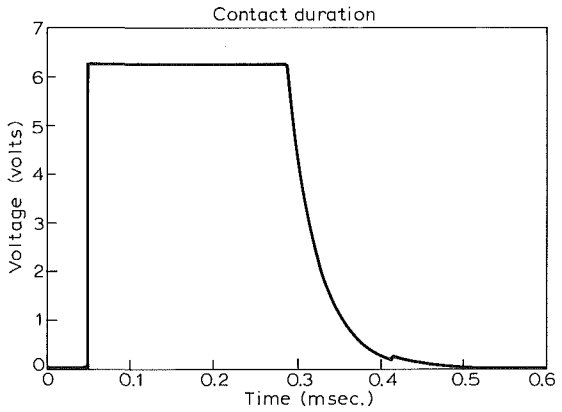

Fig. 1 Test set-up for measuring contact duration

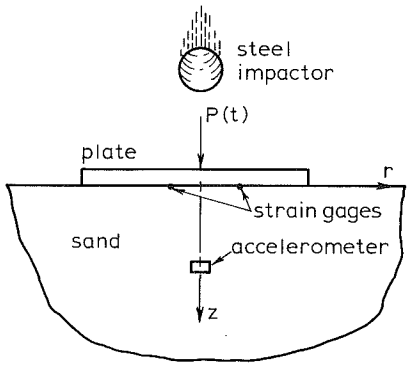

Fig. 2 Test configuration for measuring strain and acceleration

solve the dynamic response of a massless flexible circular plate with a rigid core supported on a layered viscoelastic half space subjected to harmonic vertical and rocking excitation. Krenk and Schmidt (1981) used a polynomial expansion of the contact stress and the normal displacement of the plate to obtain the response of an oscillating elastic circular plate on an elastic half space. Whittaker and Christiano (1982), who studied the dynamic behavior of rectangular plates on an elastic half space, combined the discretized Lamb's solutions with the plate treated by finite element method.

The dynamic response of an elastic plate resting on sand is a practical topic for investigation that covers a wide range of applications. First, the plate can be viewed as a footing of a structure, which has significance for foundation-vibration studies. Secondly, the finite plate response due to an impact force is a fundamental problem in structural design. Morever, investigating the impact force itself is also important and interesting since an accurate knowledge of the live load on the impacted structure enables a better design and prediction of the damage to the structure. Finally, it is important to understand fully the impact loading transmission through the soil.

Test Set-Up

For the impact test, the duration and the contact area can be predicted from a theoretical approach based on the assumptions of Hertzian contact. The impactor is a steel ball and the target is either a steel or an aluminum plate placed over Ottawa 20–30 standard sand. The test data were recorded by a Nicolet 4094 Digital oscilloscope with XF-44 Dual Disk Recorder.

The test set-up to measure the contact duration is shown in Fig. 1. By using a large resistor to increase the voltage jump, the contact duration was measured from the time of first contact with the target plate until contact was lost. The contact duration, T_o, is also shown in Fig. 1. The experimentally measured contact areas are taken as the plastic deformed region of the plate surface. The measured values of contact duration and radius of contact area are given in Table 1.

In order to understand the loading function, two strain gages were placed at the bottom of the target plate. One was placed 1.27 cm from the center of the plate and the other 1.91 cm from the center (Fig. 2). A Wheatstone Bridge Circuit was used for each strain measurement. Since the total experimental duration was within a few milliseconds, temperature compensation was not applied. The length of the strain gage was 0.8 mm.

The test set-up to determine the wave speed of the sand is shown in Fig. 3. Three piezoelectric accelerometers (Glennite Model A30T) were buried in the sand. The tank was partially filled with sand which was compacted at approximately every 5 cm. The compaction was done by 25 uniform strokes with a 24.5N hammer and 30 cm free drop. After the compaction, the total density was calculated by the measured weight and volume. The accelerometers were carefully placed and leveled in order to get excitations only in the vertical direction. The surface of the sand was covered with the target plate which was leveled. The water content of the sand was 0.05 percent. The sand was fairly condensed with a void ratio of 0.492. The accelerations were recorded after each impact by using a sampling rate of 1 μsec per point. Three to five tests were conducted for each test configuration to verify the reproducibility of the data.

The way to locate the axis of impact loading is described next. The sand bed was at a depth of about 7 cm and well compacted. An accelerometer was placed at the center of the sand bed. A plumb bob was used to aim the accelerometer; the plumbline was marked as a ruler. To ensure that the accelerometer is horizontal, a bull's-eye level was placed on its

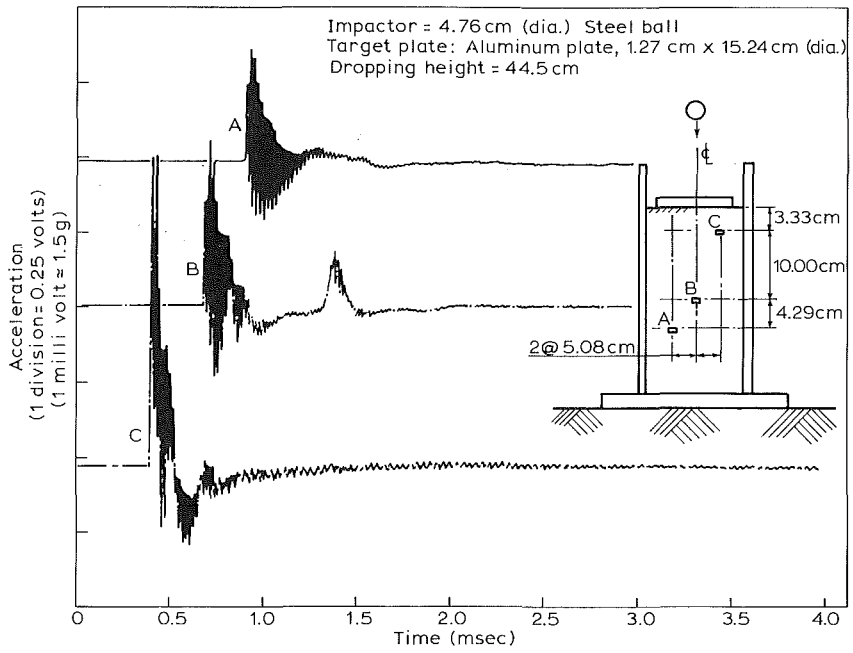

Fig. 3 Typical time history of acceleration in sand

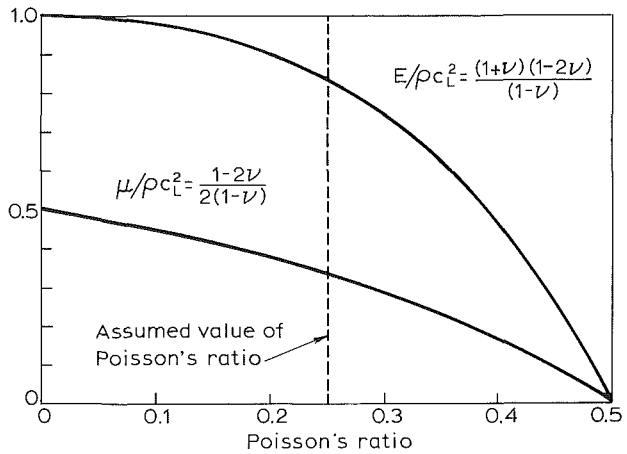

Fig. 4 Influence of Poisson's ratio

surface. Then, the plumb bob was pulled up by the plumb line through the pulley which was assumed fixed. After the accelerometer was covered by sand and the sand was compacted, an aluminum plate was used to cover the sand. The center of the plate was located by the plumb bob and this was taken as the dropping point. The plate was leveled and the dropping axis was the same as the plumb line axis.

It should be noted that after each test, the position of the accelerometer was measured again when the sand was ladled out. The accelerometer settled about 3.2 mm for each 7 cm of buried depth and caused about 5 percent error for determining the wave speed of the sand.

Analysis

To analyze the results obtained from the experimental setup as shown in Fig. 2, three modeling tasks were performed: An estimate was made of the impact loading, the interfacial conditions between the target plate and sand was determined, and the properties of the sand were evaluated. Among these three, accurate modeling of the properties of the sand is perhaps the most difficult, even in the "dry" condition.

(*a*) Modeling of the Sand. A large, short duration load applied to sand may cause it to crush, deform, slide, and change its void ratio. Such complex behavior is far beyond the capability that elasticity and viscoplastic modeling can accurately handle. Even if the properties of sand are assumed fixed within the framework of elasticity and plasticity, the sand's nonlinearity must be taken into account, since the secant modulus of sand depends highly on the stress level, loading rate, and loading history (see Kiger et al., 1984). As a consequence, when an impact which may cause a highly nonuniform stress distribution is applied, the secant shear and Young's moduli will also be highly nonuniform. Thus, an effective and efficient calculation may prove difficult to obtain. Furthermore, it is noted that unloading must be taken into account when the peak has passed.

Sand can not support tensile loads. In order to avoid the consequences of this property and strengthen the analysis, the experimental program has been designed to subject the sand only to compressive loads. By putting a plate on the surface of the sand to provide sufficient compression, the separation between the sand particles can be prevented. Thus it is assumed that no tensile force exists in the sand during the loading process.

To obtain an analytical result as a first-order approximation, sand was modeled as an elastic, isotropic, and homogeneous medium. The related elastic properties can be determined from the observed wave speed. This idea was suggested in a study by Lambe and Whitman (1969) where they evaluated the secant modulus of Ottawa sand by using the wave speed under different initial stress levels. The same concept is used here to estimate the elastic constants under the current loading rate in an average sense. Figure 3 is the recorded response of the accelerometer at various depths. From this figure, the longitudinal wave speed, C_L, can be evaluated by dividing the distance between two accelerometers by the difference of the arrival times. The shear wave speed can not be obtained since the shear wave front has not separated from the longitudinal wave in the time frame of measurements. Thus, a value for Poisson's ratio had to be assumed to evaluate the Young's modulus E and shear modulus μ. In Fig. 4, the influence of Poisson's ratio, ν, on the moduli are plotted. A summary of sand properties are given in Table 2.

(*b*) Impact Analysis. As shown in Fig. 2, the impact force to be transmitted to sand is provided from the dropped ball. The considerations on this impact force are threefold.

Table 2 Material properties

	ν	ρ (kg/m^3)	C_L (m/sec)	C_T (m/sec)	E (MPa)
Aluminum	1/3	2821 (2700)[1]	6054 (6300)[1]	3027 (3100)[1]	68928 (69192)
Ottawa[2] 20-30 Sand	1/4 (assumed)	1776 (1762)[3]	241 (256)[3]	139 (158)[4]	86 (110)

1 Achenbach, 1980
2 Void Ratio $e=0.492$
3 Lambe and Whitman, 1969
4 Richart et al., 1970

First, to study the wave phenomenon in soil-structure interaction, the impact duration, T_o, multiplied by the longitudinal wave speed of sand, should be of the same order of magnitude as the depth of the buried structure or instrument. Second, to simplify the calculation, the contact area should be small enough that the impact loading can be represented as a point load, i.e.,

$$P(r,t)=p(t)\delta(r)/2\pi r \tag{1}$$

where $\delta(r)$ is the delta function.
Finally, the point force, $p(t)$ should be able to be assumed or verified reasonably well.

From the Hertzian contact assumptions, the impact duration is given as (Timoshenko and Goodier, 1951, p. 421)

$$T_o=2.94\,(5M_b/4n)^{2/5}/(2gH)^{1/5} \tag{2}$$

where M_b is the mass of the ball; H is the dropping height, g is the value of acceleration of gravity;

$$n=\frac{4/3R_b^{1/2}}{(1-\nu_b^2)/E_b+(1-\nu_p^2)/E_p} \tag{3}$$

R_b is the radius of the ball; and E_b, ν_b, and E_p and ν_p are the Young's modulus and Poisson's ratio of the ball and the target plate, respectively. The maximum contact radius is

$$a=R_b^{1/2}(5gHM_b/2n)^{1/5} \tag{4}$$

In Table 1, the measured contact radius and contact duration are compared to those evaluated and are seen to be reasonably close to the theoretical predictions. The measured contact duration is expected to be longer than the Hertzian contact duration due to the boundary effect (Greszczuk, 1982). Since the contact radius a is much smaller than the buried depth of the accelerometer, the acceleration in the sand may be evaluated by assuming it arises from a point force on the plate. However, a is not small compared to h, the thickness of the plate, and r, the distance between the strain gage and the center of the plate. Thus, some inaccuracy is introduced when the strain is evaluated by using the point force assumption. As can be seen from Table 1, the contact duration is of the right order of magnitude for investigating the wave phenomenum in this study.

(c) Analysis of System. The target plate was relatively thick to prevent its separation from the foundation and to prevent permanent deformation in the plate except at the contact point. However, a layer model is unsuitable to analyze the target plate because the contact duration, T_o, is too long compared to the time for a longitudinal wave to travel from the top to the bottom of the plate. Thus, a thin plate model was used to simulate the response of the target plate. The governing equation is

$$D\nabla^4 w+\rho h\partial^2 w/\partial t^2=p(t)\delta(r)/2\pi r-q(r,t) \tag{4a}$$

$$D=E_p h^3/12(1-\nu_p^2) \tag{4b}$$

where D, w, and ρ are the rigidity, deflection, and density of the plate, respectively; ∇^4 is a biharmonic operator, $p(t)$ is the impact force, and $q(r, t)$ is the interfacial normal traction. The transformed solution of equation (4) has the following form:

$$\bar{w}^0=(\bar{p}/2\pi-\bar{q}^0)/D(\xi^4-\lambda^4)+B_1+B_2 \tag{5}$$

Here, a superscript bar denotes a Fourier transform and superscript zero denotes a Hankel transform, i.e.,

$$\bar{w}=\int_{-\infty}^{\infty} we^{i\omega t}dt,\quad \bar{w}^0=\int_0^{\infty}\bar{w}J_o(\xi r)rdr \tag{6),(7}$$

and

$$\lambda^4=\rho\omega^2 h/D \tag{8}$$

The terms B_1 and B_2, can be determined from the boundary conditions of the target plate, i.e., vanishing shear force and bending moment at $r=R$.

$$\frac{\partial}{\partial r}\left(\frac{\partial^2\bar{w}}{\partial r^2}+\frac{1}{r}\frac{\partial\bar{w}}{\partial r}\right)\Big|_{r=R}=0 \tag{9}$$

$$\left(\frac{\partial^2\bar{w}}{\partial r^2}+\nu_p\frac{1}{r}\frac{\partial\bar{w}}{\partial r}\right)\Big|_{r=R}=0 \tag{10}$$

Next, the transfer of load into the sand is considered. Two extra interfacial conditions were assumed. First, no separation was assumed between the plate and sand, leading to continuous normal traction and displacement across the interface. Next, the friction force between the plate and sand was assumed negligible when compared to the interfacial normal traction. This condition could be modified, for example, by assuming that the interfacial shear force is proportional to the interfacial normal force.

The response in the elastic half space due to a normal traction applied on the surfaces is Lamb's problem. The transformed normal displacement in sand due to q is

$$\bar{w}^0=\bar{q}^0(\alpha/\mu\Omega)[(2\xi^2-k_T^2)e^{-\alpha z}-2\xi^2 e^{-\beta z}] \tag{11}$$

where,

$$\alpha=(\xi^2-k_L{}^2)^{1/2} \tag{11a}$$

$$\beta=(\xi^2-k_T{}^2)^{1/2} \tag{11b}$$

$$\Omega=(2\xi^2-k_T{}^2)^2-4\xi^2\alpha\beta \tag{11c}$$

$$k_L=\omega/C_L \tag{11d}$$

$$K_T=\omega/C_T \tag{11f}$$

C_L and C_T are the longitudinal and shear wave speeds in the sand.

The interfacial traction $\bar{q}^0$ can be obtained by eliminating $\bar{w}^o$ in equation (5) and equation (11). The result is

$$\bar{q}^0=\frac{\mu\Omega}{\mu\Omega-k_T^2\alpha D(\xi^4-\lambda^4)}\left[\frac{\bar{P}}{2\pi}+(B_1+B_2)D(\xi^4-\lambda^4)\right] \tag{12}$$

It should be noted that B_1 and B_2 contain the integral form of $\bar{q}$. Hence a numerical method must be used to solve for $\bar{q}^o$.

However, as a first order approximation, R was assumed so large (infinite plate) that B_1 and B_2 approach 0. If R is considered as moderately large, $\bar{q}^o$ may be obtained by the method of substitution. Whether R can be considered large enough depends also on the range of the loading frequency. After $\bar{q}^o$ is obtained, $\bar{w}^0$ is evaluated via equation (11) and $\bar{q}$ is obtained by evaluating the Hankel integral. The numerical value of acceleration of sand in the frequency domain is $-\omega^2\bar{w}$. Also, the strain along the bottom of the plate can be evaluated by the following formula:

$$\bar{\epsilon}_r = -\frac{h}{2}\frac{\partial^2 \bar{w}}{\partial r^2} \tag{13}$$

Numerical and Experimental Results

(a) Radial Strain on the Plate. The first part of the numerical results is the computation of the Green's function of strain along the bottom of the plate. Mathematically, the strain caused by the impact force is written as:

$$\bar{\epsilon}_r(r, \omega) = G(r, \omega) * \bar{p}(\omega) \tag{14}$$

where G is the Green's function. In Fig. 5, the spectrum of $|G(r,\omega)|$ is plotted at various locations along the bottom of an aluminum plate with $h = 1.27$ cm and $R = \infty$. The strain at $r = 0$ is not plotted because the deflection due to a point load contains a $r^2\log(r)$ term, thus, the strain at $r = 0$ has a logarithmic singularity. Strain gages were put at $r = 1.27$ cm and 1.91 cm such that the following conditions were met: $a \cong 0.2$ cm $< h = 1.27$ cm $\leq r \ll R = 7.62$ cm. The influence of the size of strain gages and the deviation of impact point in the experiment are not important because they are smaller than the maximum contact radius. For the static case of an infinite plate rested on an elastic half space, there is an integral form available for the deflection curve from Timoshenko and Woinowsky-Krieger (1959).

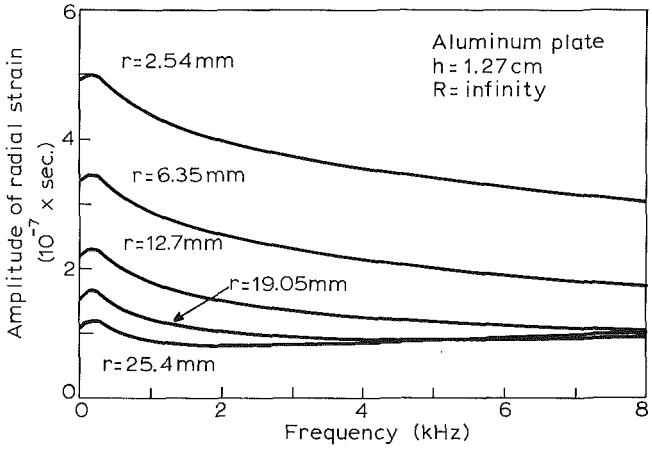

Fig. 5 Spectrum of radial strain due to a point force

$$w(r) = \frac{Pl_0^2}{2\pi D}\int_0^\infty \frac{J_0(\zeta r/l_0)}{1+\zeta^3}d\zeta, \tag{15}$$

where,

$$l_0^3 = \frac{2D(1-\nu^2)}{E}$$

After differentiating the Bessel function twice with respect to r, the strain can be evaluated; this evaluation provides a check of the numerical results at $\omega = 0$. Also, it is noted that the ratio of the amplitude of the strain at $r = 76.2$ mm (calculated but not shown in Fig. 5) to the strain at $r = 12.7$ mm is only 0.11 at $\omega = 0$, which implies that the infinite plate assumption is valid for the static case. Next, the curves in Fig. 5 are ascending as the frequency slightly increases because there is a pole along the positive real axis at a frequency of 350 Hz. Finally, it is observed that the boundary effect becomes larger as the frequency becomes higher. At frequency equal to 4 kHz, the ratio of amplitude of the strain at $r = 76.2$ mm to the strain at $r = 12.7$ mm is 0.75.

Since $G(r,\omega)$ is based on several assumptions such as point impact, an infinite plate, and a frictionless interfacial condition along with uncertainties in soil properties, to invert $p(t)$ from the strain gage measurement is not reliable. Consequently, $p(t)$ is estimated in the following way. First, assume

$$p(t) = Af(t) \tag{16a}$$

where $f(t)$ is a monopeak, nonzero smooth shape function in the interval $0 < t < T_0$. Then, the amplitude, A, is determined from a momentum balance, i.e.,

$$A = M_b(2gH)^{1/2} \Big/ \int_0^{T_0} f(t)dt \tag{16b}$$

In Fig. 6, three $f(t)$ curves are plotted. The curve No. 1 is the Hanning function. The curve No. 2 is recommended by

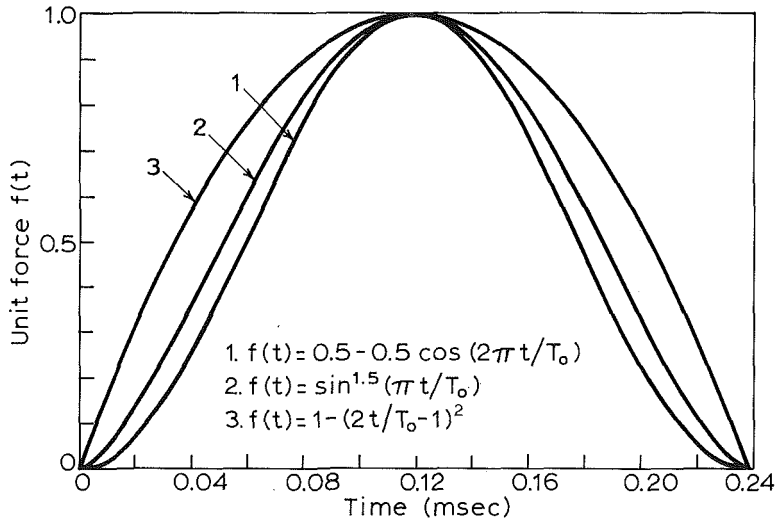

Fig. 6 Loading shape function

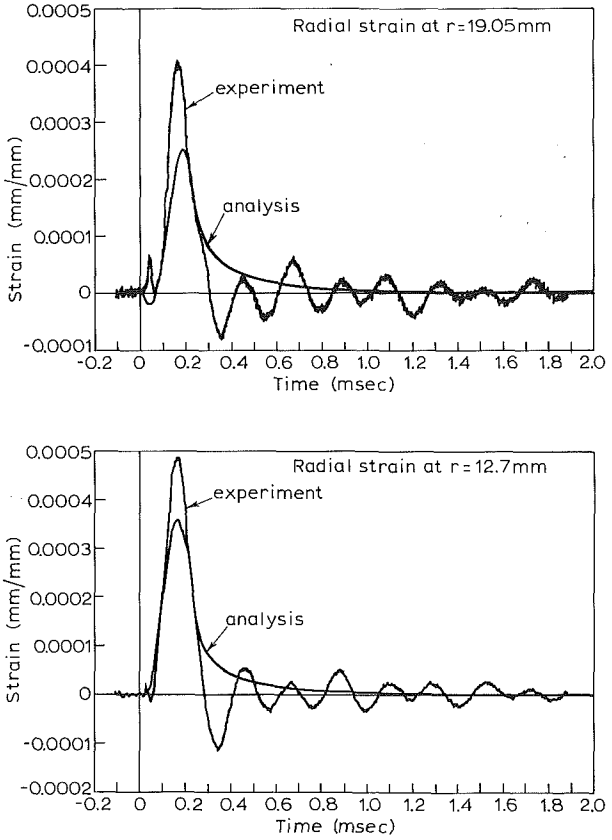

Fig. 7 Comparison of simulated strains with experimental results

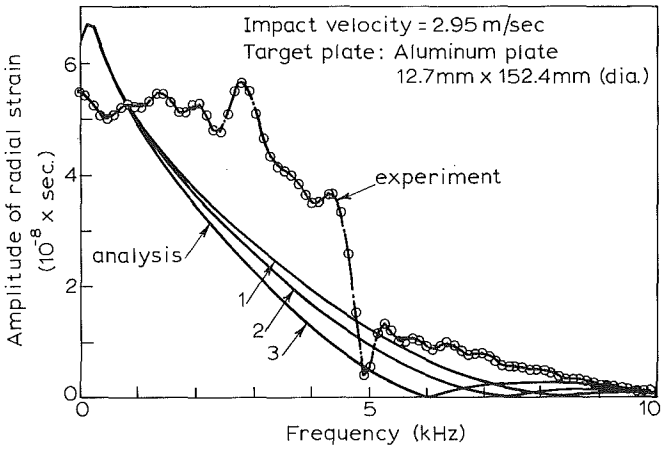

Fig. 8 Spectrum of strain at $r = 1.27$ cm

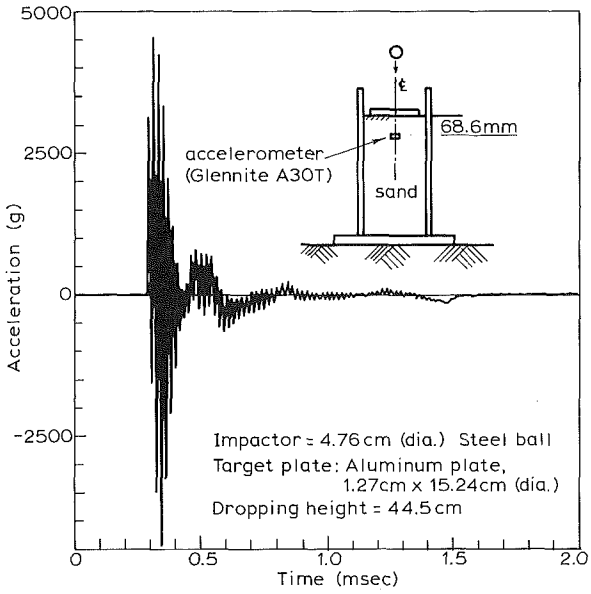

Fig. 9 Measured acceleration history

Gresczuk (1982) to approximate the Hertzian contact force. The curve No. 3 is the parabolic function. It is noted that the first two curves are very close.

Next, the impact of a steel ball dropped from $H = 44.5$ cm, hitting an aluminum plate $h = 1.27$ cm and $R = 7.62$ cm, is considered. The impact duration is 0.238 msec and the amplitude is evaluated via equation (16*b*). From $p(t)$, the Fourier transform $\bar{p}(\omega)$ is evaluated and multiplied with the Green's function. Thus, the numerical result for the strain in the frequency domain is obtained. After applying the inverse Fast Fourier Transform, the time domain response is obtained. In Fig. 7, the measured strain histories at $r = 1.27$ cm and $r = 1.91$ cm are plotted and compared with the simulated strains assuming $f(t)$ is the Hanning function. The general agreement is satisfactory. The oscillations in the experimental results are due to the finite plate vibration.

To obtain the spectrum of measured strain, FFT was applied to the experimental results. At $\omega = 0$, there is good agreement between experimental results and numerical results (Fig. 8). As was mentioned previously, the infinite plate assumption is valid in static cases. It should be noted that all three numerical curves corresponding with three $f(t)$ from Fig. 6, have the same value at $\omega = 0$ because they have to satisfy momentum balance. However, there are large differences between the numerical results and experimental results between about 2 to 5 kHz range. The reason is that the numerical results are evaluated using an infinite plate assumption while the experimental results are for a finite plate. If the finite plate vibration is considered, the natural frequency of the plate is of the form

$$\omega = \eta^2 \left(\frac{D}{\rho_p h R^4} \right)^{1/2} \tag{17}$$

where η^2 is a constant which depends only on the boundary conditions at $r = R$. For a completely free circular plate, the first root $\eta^2 = 9.084$ (Leissa, 1961) with corresponding frequency of 4.78 kHz is the same as the frequency of the oscillation which was observed after the loading (Fig. 7). To determine $f(t)$ more accurately, a finite plate analysis must be performed.

(*b*) Acceleration in the Sand. The next set of results describe the acceleration in the sand. The impactor is a 4.76 cm diameter steel ball and is dropped from $H = 44.5$ cm. The target plate is an aluminum plate with $h = 1.27$ cm and $R = 7.62$ cm. Only the Hanning function is considered for the loading shape function. The testing geometry was similar as shown in Fig. 3. The accelerometers A and C were removed and reburied B at depth $d = 6.86$ cm. Figure 9 is the record of acceleration. The corresponding spectrum is plotted in Fig. 10.

The Glennite Model A30T piezoelectric accelerometer is a general-purpose accelerometer for shock acceleration measurement from a fraction of 10 g to 10,000 g. It was calibrated with a response of 1.46 g/mv. The size of the accelerometer is 1.8 cm × 2.5 cm × 2.5 cm and its natural frequency is 50 kHz. The basic difficulty in choosing the accelerometer for this experiment is that the size of the accelerometer must be very small; otherwise, a large scale test must be performed. However, due to its availability and con-

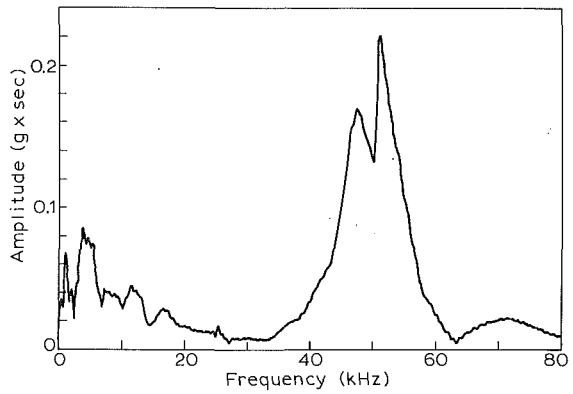

Fig. 10 Complete spectrum of measured acceleration

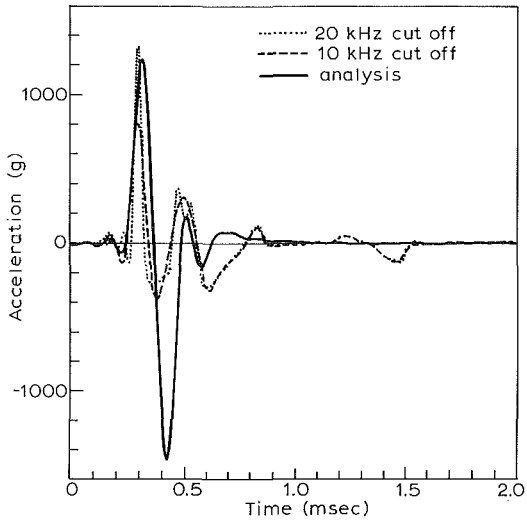

Fig. 11 Simulated acceleration and measured acceleration

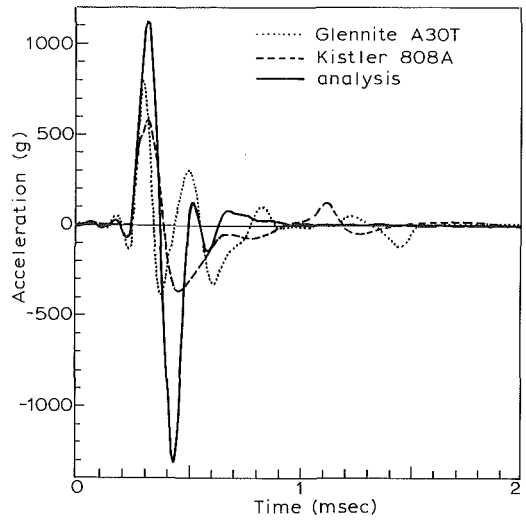

Fig. 12 Acceleration measured from different accelerometers

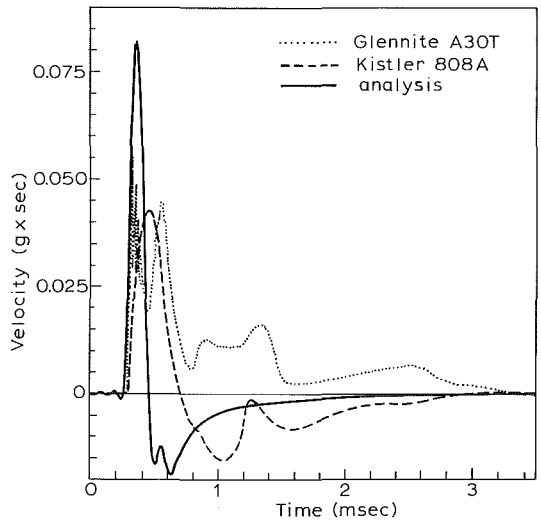

Fig. 13 Simulated velocity history and integrated velocity history

venience, the Glennite A30T was used in measuring the wave speed of the sand. It is noted that the arrival time was distinct (Fig. 3) and the response of accelerometer was within the right order of magnitude. In Fig. 11, the simulated acceleration and the measured acceleration are plotted. For the dotted line, the frequency above 20 kHz has been filtered out; for the dashed line, the frequency above 10 kHz has been filtered. It is noted that the peak positive acceleration is quite sensitive to the cutoff frequency and the experimental result is comparable to its numerical simulation.

It was noted from the strain measurement (Fig. 8) that the frequency range of the impact loading was within 10 kHz. Therefore, the 50 kHz noise in the acceleration measurements (shown in Fig. 10) implied some problems with accelerometer. In Fig. 12, the simulated acceleration history and the measured acceleration history obtained by a different accelerometer are plotted. A smaller accelerometer was used. The Kistler model 808A Quartz accelerometer with a size of 1.27 cm (hex.) $\times$ 2.29 cm is a general purpose piezoelectric accelerometer for vibration, shock and acceleration measurements with a full scale range from 1 g to 10,000 g. By using this accelerometer, the measured acceleration in frequency domain shows almost no amplitude after 10 kHz. This coincided with the strain measurements.

There are three points to be noted in Fig. 12. First, the arrival time of the simulated acceleration is quite satisfactory, which provides an indirect check of the simulated acceleration spectrum. Second, the acceleration is very small after 1.6 msec for all 3 curves. This coincides with the duration measured by the strain gages. Finally, the numerical peak negative acceleration is quite close to the peak positive acceleration, while the measured peak negative acceleration is significantly less than the peak positive acceleration. Since negative acceleration means the velocity is decreasing as are the stresses, the negative acceleration period is an unloading period. Thus, the significant reduction in measured peak negative acceleration implies that the stress-strain relationship in the unloading phase may be quite different from the loading phase. Therefore, the current linear elastic assumption may be violated. This last point can be clarified after the finite plate analysis is performed.

In Fig. 13, the velocity histories, which are obtained from the integration of simulated and measured accelerations without filtering out any frequency component, are plotted. As a check, all three velocity curves become 0 at around 3 msec. In Fig. 14, the spectrums of simulated acceleration and measured accelerations are plotted. The agreement is good at frequencies up to 1.5 kHz. It may be possible to have better correlation between the experimental and numerical results by introducing attenuation into the analysis. The wave speed in sand is 240 m/s and as the frequency increases to 10 kHz, the wave length in sand can be as short as 2.4 cm. Since the accelerometer is apparently too large, a better calculation may be done by considering a scattering problem.

The current analytical approach can provide a reliable strain

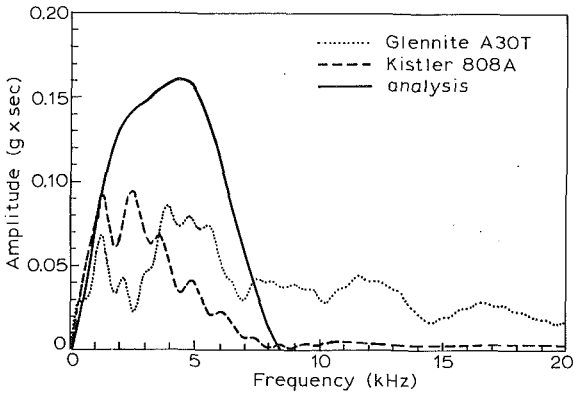

Fig. 14 Simulated spectrum and experimental spectrum

history and acceleration history within the same order of magnitude in comparison with the experimental results. The major errors arise from the infinite plate assumption and the dimensions of instruments used to measure acceleration in the sand.

Summary

In this paper, the basic approach was expressed. The main objective is to understand the physical phenomena. The *arrival time*, *duration*, and *magnitude* have good correlation between the analysis and experiment. The overall results are reasonably good and provide an understanding of the transmission of impact load through the plate, the interaction between the plate and the sand, and the propagation of the load into the sand.

The following conclusions can be made at this point:

1 Using the current approach, numerical results are comparable to experimental results. The accuracy is within the same order of magnitude.
2 To get a better estimate of the impact loading, it is necessary to consider finite plate effects.
3 The accelerometer size effect is not negligible in current testing scales.
4 The errors from the assumptions of interfacial conditions and point impact are much smaller than the errors from (2) and (3). The effect of an assumed Poisson's ratio on soil response needs further investigation.
5 Attenuation may be introduced to compensate for the energy consumed on sliding (internal friction between soil particles).

Acknowledgment

The authors are grateful for support from the Air Force Office of Scientific Research. They are pleased to acknowledge the Program Manager, Directorate of Aerospace Sciences, Major Steven C. Boyce and former Program Manager Dr. Spencer T. Wu.

References

Achenbach, J. D., 1980, *Wave Propagation in Elastic Solids*, North-Holland Publishing Co., Amsterdam.

Achenbach, J. D., Keshava, S. P., and Herrmann, G., 1966, "Waves in a Smoothly Joined Plate and Half Space," *Journal of the Engineering Mechanics Division, Proceedings*, ASCE, Vol. 92, No. EM2, pp. 113-129.

Al-Mousawi, M. M., 1986, "On Experimental Studies of Longitudinal and Flexural Wave Propagations: An Annotated Bibliography," *Applied Mechanics Reviews*, ASME, Vol. 39, No. 6, pp. 853-865.

Arnold, R. N., Bycroft, G. N., and Warburton, G. B., 1955, "Forced Vibrations of a Body on an Infinite Elastic Solid," ASME JOURNAL OF APPLIED MECHANICS, Vol. 22, pp. 391-400.

Bycroft, G. N., 1956, "Forced Vibrations of a Rigid Circular Plate on a Semi-Infinite Elastic Space and on an Elastic Stratum," *Phil. Transactions Royal Society London*, Vol. A248, pp. 327-368.

Collins, W. D., 1962, "The Forced Torsional Oscillations of an Elastic Half-Space and an Elastic Stratum," *Proceedings of London Mathematical Society*, Vol. 12, pp. 226-244.

Freund, L. B., and Achenbach, J. D., 1968, "Waves in a Semi-Infinite Plate in Smooth Contact With a Harmonically Disturbed Half Space," *International Journal of Solids and Structures*, Vol. 4, pp. 605-621.

Greszczuk, L. B., 1982, "Damage in Composite Materials Due to Low Velocity Impact," *Impact Dynamics*, J. A. Zukas et al., eds., John Wiley, New York.

Iguchi, M., and Luco, J. E., 1982, "Vibration of Flexible Plate on Viscoelastic Medium," *Journal of the Engineering Mechanics Division, Proceedings*, ASCE, Vol. 108, No. EM6, pp. 1103-1120.

Karasudhi, P., Keer, L. M., and Lee, S. L., 1968, "Vibratory Motion of a Body on an Elastic Half-Plane," ASME JOURNAL OF APPLIED MECHANICS, Vol. 35, pp. 697-705.

Kiger, S. A., Getchell, J. V., Slawson, T. R., and Hyde, D. W., 1980-1984, "Vulnerability of Shallow-Buried Flat Roof Structures," US Army Engineer Waterways Experiment Station, Technical Report SL-80-7, six parts.

Krenk, S., and Schmidt, H., 1981, "Vibration of an Elastic Circular Plate on an Elastic Half Space—A Direct Approach," ASME JOURNAL OF APPLIED MECHANICS, Vol. 48, pp. 161-168.

Lamb, H., 1904, "On the Propagation of Tremors over the Surface of an Elastic Solid," *Philosophy Transactions Royal Society London, Ser. A*, Vol. 203, pp. 1-42.

Lambe, T. W., and Whitman, R. V., 1969, *Soil Mechanics*, John Wiley, New York.

Leissa, A. W., 1969, "Vibration of Plates," NASA Report No. SP-160.

Lin, Y. J., 1978, "Dynamic Response of Circular Plates Resting on Viscoelastic Half-Space," ASME JOURNAL OF APPLIED MECHANICS, Vol. 45, pp. 379-384.

Luco, J. E., and Mita, A., 1987, "Response of a Circular Foundation on a Uniform Half-Space to Elastic Waves," *Earthquake Engineering and Structural Dynamics*, Vol. 15, pp. 105-118.

Luco, J. E., and Westmann, R. A., Oct. 1971, "Dynamic Response of a Circular Footings," *Journal of the Engineering Mechanics Division, Proceedings*, ASCE, No. EM5, pp. 1381-1395.

Luco, J. E., and Westmann, R. A., 1972, "Dynamic Response of a Rigid Footing Bonded to an Elastic Half-Space," ASME JOURNAL OF APPLIED MECHANICS, Vol. 39, pp. 527-534.

Oien, M. A., 1973, "Steady Motion of a Plate on an Elastic Half-Space," ASME JOURNAL OF APPLIED MECHANICS, Vol. 40, Series E, No. 2, pp. 478-484.

Quinlan, P. M., 1954, "The Elastic Theory of Soil Dynamics," *Symposium on Dynamic Testing of Soils*, ASTM, STP No. 156, pp. 3-34.

Reissner, E., and Sagoci, H. F., 1944, "Forced Torsional Oscillations of an Elastic Half-Space," *Journal of Applied Mechanics*, Vol. 15, pp. 652-662.

Richard, Jr., F. E., Hall, Jr., J. R., and Woods, R. D., 1970, *Vibrations of Soils and Foundations*, Prentice-Hall, Englewood Cliffs, N.J.

Robertson, I. A., 1966, "Forced Vertical Vibration of a Rigid Circular Disc on a Semi-Infinite Elastic Solid," *Proceedings of Cambridge Philosophy Society*, Vol. 62, pp. 547-553.

Sung, T. Y., 1954, "Vibrations in Semi-Infinite Solids Due to Periodic Surface Loadings," *Symposium on Dynamic Testing of Soils*, ASTM, STP No. 156, pp. 35-64.

Timoshenko, S., and Goodier, J. N., 1970, *Theory of Elasticity*, 3rd Ed., McGraw-Hill, New York.

Timoshenko, S., and Woinowsky-Krieger, S., 1959, *Theory of Plates and Shells*, McGraw-Hill, New York.

Veletsos, A. S., and Verbic, B., 1974, "Basic Response Functions for Elastic Foundations," *Journal of the Engineering Mechanics Division, Proceedings*, ASCE, Vol. 100, No. EM2, pp. 189-202.

Whittaker, W. L., and Christiano, P., 1982, "Dynamic Response of Flexible Plates on Elastic Half-Space," *Journal of the Engineering Mechanics Division*, ASCE, Vol. 108, pp. 133-154.